Proc. Natl. Acad. Sci. USA
Vol. 89, pp. 5675–5679, June 1992
Neurobiology

Dynamic magnetic resonance imaging of human brain activity during primary sensory stimulation

KENNETH K. KWONG†, JOHN W. BELLIVEAU†, DAVID A. CHESLER†, INNA E. GOLDBERG†, ROBERT M. WEISSKOFF†, BRIGITTE P. PONCELET†, DAVID N. KENNEDY†, BERNICE E. HOPPEL†, MARK S. COHEN†, ROBERT TURNER‡, HONG-MING CHENG§, THOMAS J. BRADY†, AND BRUCE R. ROSEN†

†MGH–NMR Center, Department of Radiology, Massachusetts General Hospital and Harvard Medical School, Charlestown, MA 02129; ‡National Institutes of Health, Laboratory of Cardiac Energetics, National Heart, Lung, and Blood Institute, Bethesda, MD 20892; and §Howe Laboratory of Ophthalmology, Massachusetts Eye and Ear Infirmary and Harvard Medical School, Boston, MA 02114

Communicated by David H. Hubel, March 26, 1992

ABSTRACT **Neuronal activity causes local changes in cerebral blood flow, blood volume, and blood oxygenation. Magnetic resonance imaging (MRI) techniques sensitive to changes in cerebral blood flow and blood oxygenation were developed by high-speed echo planar imaging. These techniques were used to obtain completely noninvasive tomographic maps of human brain activity, by using visual and motor stimulus paradigms. Changes in blood oxygenation were detected by using a gradient echo (GE) imaging sequence sensitive to the paramagnetic state of deoxygenated hemoglobin. Blood flow changes were evaluated by a spin-echo inversion recovery (IR), tissue relaxation parameter T_1-sensitive pulse sequence. A series of images were acquired continuously with the same imaging pulse sequence (either GE or IR) during task activation. Cine display of subtraction images (activated minus baseline) directly demonstrates activity-induced changes in brain MR signal observed at a temporal resolution of seconds. During 8-Hz patterned-flash photic stimulation, a significant increase in signal intensity (paired t test; $P < 0.001$) of 1.8% ± 0.8% (GE) and 1.8% ± 0.9% (IR) was observed in the primary visual cortex (V1) of seven normal volunteers. The mean rise-time constant of the signal change was 4.4 ± 2.2 s for the GE images and 8.9 ± 2.8 s for the IR images. The stimulation frequency dependence of visual activation agrees with previous positron emission tomography observations, with the largest MR signal response occurring at 8 Hz. Similar signal changes were observed within the human primary motor cortex (M1) during a hand squeezing task and in animal models of increased blood flow by hypercapnia. By using intrinsic blood–tissue contrast, functional MRI opens a spatial–temporal window onto individual brain physiology.**

The brain possesses anatomically distinct processing regions. A complete understanding of brain function requires determination of where these sites are located, what operations are performed, and how distributed processing is organized (1). Changes in neuronal activity are accompanied by focal changes in cerebral blood flow (CBF) (2), blood volume (CBV) (3, 4), blood oxygenation (3, 5), and metabolism (6, 7). These physiological changes can be used to produce functional maps of component mental operations.

Conventional magnetic resonance imaging (MRI) examinations provide high spatial-resolution anatomic images primarily based on contrast derived from the tissue-relaxation parameters T_1 and T_2. Recently, several investigators have demonstrated in animals that brain tissue relaxation is influenced by the oxygenation state of hemoglobin (a T_2^* effect, modulated by the local blood volume) (8–13) and intrinsic tissue perfusion (T_1 effect) (14–16). High-speed MRI techniques sensitive to these relaxation phenomena can thus be used to generate tomographic images of brain activity (17).

We report here completely noninvasive MRI of brain activity by techniques with intrinsic sensitivity to CBF and blood oxygenation state. Time-resolved MR mapping of human primary visual (V1) and motor (M1) cortex during task activation is demonstrated at a temporal resolution of seconds. The methods described here can be applied repeatedly in normal subjects with complete safety, expanding the spatial–temporal window of *in vivo* brain investigation (18).

METHODS AND RESULTS

Seven normal subjects underwent dynamic NMR imaging with a prototype high-speed imaging device (1.5 tesla; General Electric Signa; modified by Advanced NMR Systems, Wilmington, MA) based on a variation of the echo planar imaging technique (19) first described by Mansfield (20). Using a single radio frequency (rf) excitation pulse, complete two-dimensional NMR images can be acquired in <50 ms. A gradient echo (GE) imaging sequence sensitive to variations in T_2^* (repetition time between images, TR = 3000 ms; echo time, TE = 40 ms) and a T_1-sensitive spin-echo inversion recovery (IR) pulse sequence (inversion time, TI = 1100 ms; TR = 3500 ms; TE = 42 ms) were used.

The expected changes in image signal intensity due to blood flow and oxygenation-related contrast mechanisms are small (11, 14, 15). To visualize these subtle signal changes, we used a sequential task-activation paradigm, alternating between resting and stimulated states. Focal regions of cortical activation were revealed by magnitude subtraction of averaged baseline (resting) images from all subsequent images. Typically, a series of 80 images were acquired in continuous succession with the same imaging pulse sequence (either GE or IR) during rest and stimulation. The V1 of our normal volunteers was evaluated by using well-established patterned-flash photic stimulation (21, 22). Light-proof stimulating goggles (model S10VS; Grass) were placed over the subject's eyes. Each eyepiece contains a 5 × 6 rectangular array of red light-emitting diodes. Special care was taken to minimize subject movement between scans by using a snugly fitting head holder. A receive-only rf surface coil was used to improve signal/noise ratio (similar results were obtained, albeit with reduced signal/noise ratio, using a quadrature head volume coil). A single 10-mm slice with 3 × 3 mm in-plane resolution (full width at half maximum) was positioned along the banks of the calcarine fissures (4).

Fig. 1 displays real-time images in subtraction format during darkness and during 8-Hz photic stimulation. During

The publication costs of this article were defrayed in part by page charge payment. This article must therefore be hereby marked "*advertisement*" in accordance with 18 U.S.C. §1734 solely to indicate this fact.

Abbreviations: MRI, magnetic resonance imaging; GE, gradient echo; IR, inversion recovery; PET, positron emission tomography; CBV, cerebral blood volume; CBF, cerebral blood flow.

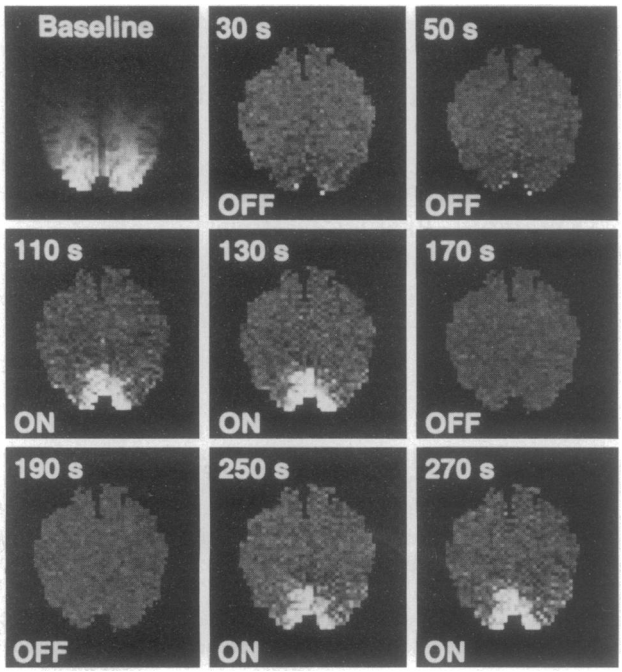

FIG. 1. Noninvasive, real-time MRI mapping of V1 activation during visual stimulation. Images are obliquely aligned along the calcarine fissures with the occipital pole at the bottom. Images were acquired at 3.5-s intervals using an IR sequence (80 images total). A baseline image acquired during darkness (*Upper Left*) was subtracted from subsequent images. Eight of these subtraction images are displayed, chosen when the image intensities (see Fig. 2) reached a steady-state signal level, during darkness (OFF) and during 8-Hz photic stimulation (ON). During stimulation, local increases in signal intensity are detected in the medial–posterior regions of the occipital lobes along the calcarine fissures.

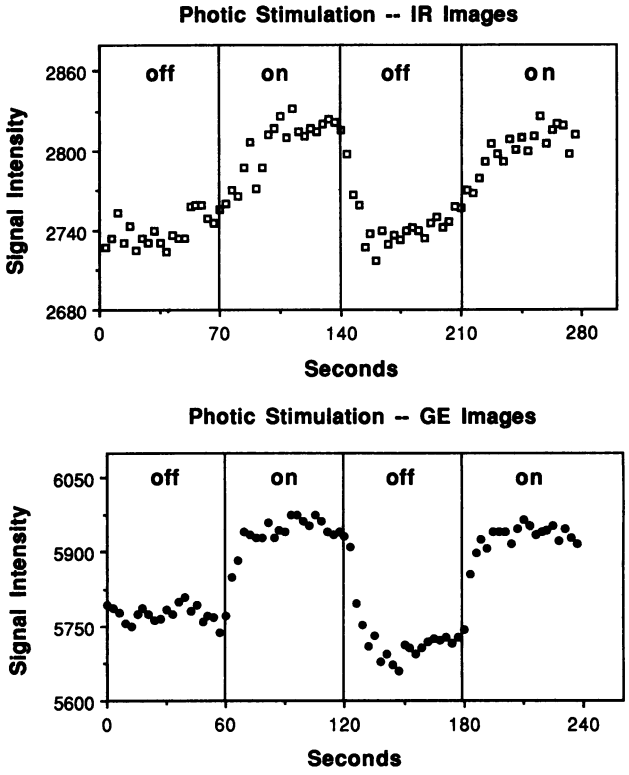

FIG. 2. Signal-intensity changes for a region of interest (≈60 mm²) within the visual cortex during darkness and during 8-Hz photic stimulation. Results using both IR (flow sensitive) and GE (oxygenation sensitive) techniques are shown. The T_1-weighted IR data (subtraction images shown in Fig. 1) were collected once every 3.5 s, and the T_2^*-weighted GE data were collected once every 3 s. Brain signal change for this particular subject is ≈3% for both IR and GE acquisitions. Upon termination of photic stimulation, an undershoot in GE signal intensity is observed, consistent with known physiological oxygenation and pH changes.

photic stimulation, each of our subjects showed a significant increase in signal intensity (paired t test; $P < 0.001$) within the anatomically defined V1, with an average ($n = 7$) increase of 1.8% ± 0.8% using GE sequences and 1.8% ± 0.9% using IR sequences. The similarity between these changes is coincidental and depends on the exact choice of pulse sequence parameters, static magnetic field strength, etc. The loci and spatial extent of activated cortex correspond with previous MRI CBV maps of V1 (4). Region of interest analysis of such images is shown in Fig. 2, which demonstrates the temporal response of V1 signal intensity using both GE and IR techniques. The rise times of activation were fit to a monoexponential approach to equilibrium [$A(1 - e^{-kt})$ where t is time and A is a constant]. The mean time constant k was 4.4 ± 2.2 s for the GE images and 8.9 ± 2.8 s for the IR images.

To demonstrate further that the observed changes were physiologically based, several additional experiments were performed. First, animal experiments with rabbits using a previously described hypercapnia model (known to increase brain blood flow) (23) demonstrated an ≈4% increase in MR signal when arterial P_{CO_2} was raised from normal to hypercapnic values (Fig. 3) for both GE and IR protocols. In a second study, the known relationship between visual stimulation frequency and brain response was tested in our human volunteers with both IR and GE sequences. Fig. 4 shows a plot of MR signal response versus photic stimulation frequency. The greatest signal change occurred at 8 Hz, in agreement with previous positron emission tomography (PET) observations (21, 22). Finally, these results are not unique to the striate cortex. In two subjects, we investigated M1. Fig. 5 shows the subtraction image and time series data from an oblique coronal slice through the precentral gyrus acquired during a repetitive contralateral hand squeezing task. The activated region corresponds to the expected homuncular position within M1 (24). Cortical temporal response was similar to that observed within V1.

DISCUSSION

Our data demonstrate that the hemodynamic alterations that accompany neuronal activation lead to subtle but readily

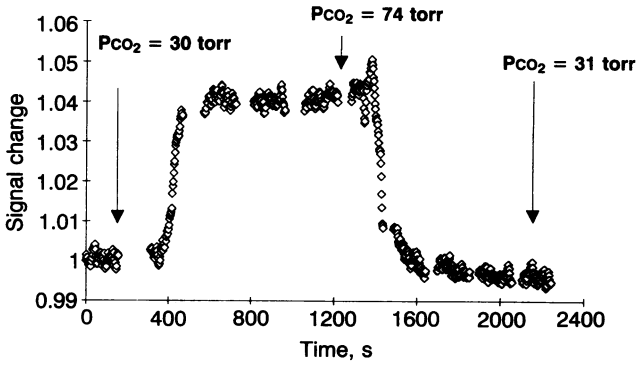

FIG. 3. Time course of rabbit brain GE signal intensity in response to changing arterial P_{CO_2}. Gated GE echo planar imaging sequence with TR ≈ 3 s and TE = 60 ms was used. Animal was imaged breathing 100% O_2 for 6.5 min, followed by ventilation with 10% CO_2/90% O_2 for the next 17 min, and finally returned to breathing 100% O_2. MR signal changes follow changes in blood P_{CO_2}, known to be linearly correlated with blood flow changes over this range of arterial P_{CO_2}s.

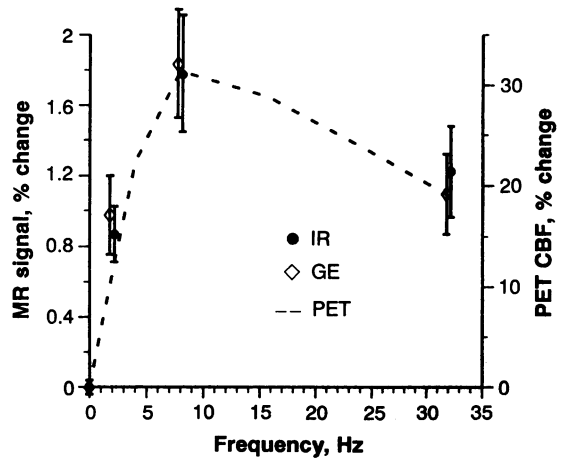

FIG. 4. MRI GE and IR signal response in striate cortex as a function of the frequency of light stimulus (0 Hz = darkness). Signal response is expressed as percentage change from baseline unstimulated level. The largest observed response occurred at 8 Hz for both techniques (IR and GE data points are graphically offset for clarity). Error bars indicate ±1 SEM (n = 5 for 2 and 32 Hz; n = 7 for 0 and 8 Hz). For comparison, CBF % change data obtained by PET and the identical stimulation paradigm [adapted from Fox and Raichle (21, 22)] at 0, 1, 4, 8, 16, and 32 Hz are superimposed on the MR data.

detectable changes on T_1- and T_2^*-weighted echo planar MR images. Flow-sensitive images show increased perfusion with activation, while our susceptibility-sensitive images show changes consistent with an increase in venous blood oxygenation. Although the precise biophysical mechanisms responsible for the signal changes have yet to be determined, good hypotheses exist to account for our observations.

T_2^* changes reflect the interplay between changes in CBF, CBV, and oxygenation. In general, MR signal loss on T_2^*-weighted images reflects magnetic field heterogeneity within

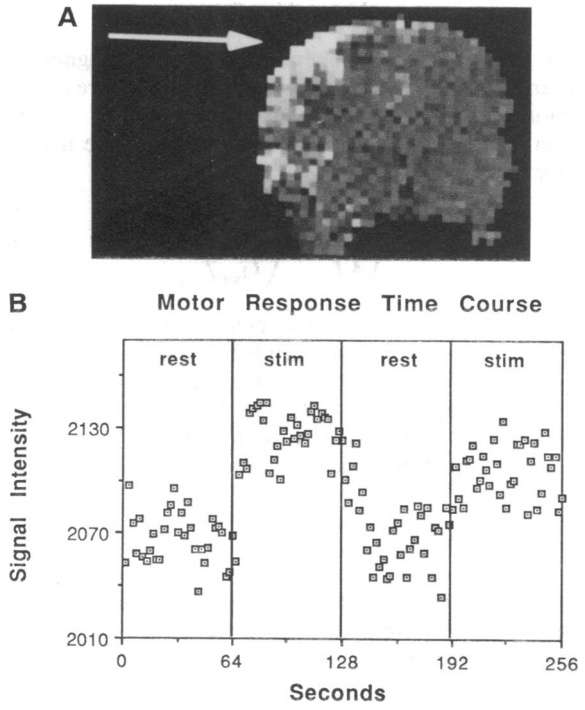

FIG. 5. (*A*) M1 activation (arrow) during repetitive contralateral hand squeezing. This coronal subtraction image (stimulated minus unstimulated) was acquired by a GE technique (TR = 2000 ms; TE = 60 ms) with the image plane obliquely aligned along the precentral gyrus. (*B*) Temporal response.

an imaging voxel. As hemoglobin becomes deoxygenated, it becomes more paramagnetic than the surrounding tissue and thus creates a magnetically inhomogeneous environment. The observed increased signal on T_2^*-weighted images during activation reflects a decrease in deoxyhemoglobin content—i.e., an increase in venous blood oxygenation. Oxygen delivery, CBF, and CBV all increase with neuronal activation. Because CBF (and hence oxygen delivery) changes exceed CBV changes by 2–4 times (25), while blood oxygen extraction increases only slightly (3, 5), the total paramagnetic blood deoxyhemoglobin content within brain tissue voxels will decrease with brain activation, even though the volume of blood increases. The resulting decrease in the tissue–blood magnetic susceptibility difference leads to less intravoxel dephasing within brain tissue voxels and hence increased signal on T_2^*-weighted images (11, 17). This observation is the converse of the decreased T_2^*-weighted signal observed by several groups during respiratory challenges known to decrease blood oxygen content (8–13, 26). Our results independently confirm PET observations that activation-induced changes in blood flow and volume are accompanied by little or no increase in tissue oxygen consumption (3, 5, 7).

The magnitude of the observed signal changes is in good agreement with recent theoretical modeling. With photic stimulation, assuming blood volume increases by 30% (4), and blood flow increases by 70%, an initial venous oxygenation of 60% with constant oxygen consumption (3, 5, 7) will give a final venous oxygenation of 75%. Since the volume susceptibility difference ($\Delta\chi$) between totally deoxygenated blood and the surrounding brain is $\approx 6.4 \times 10^{-8}$ (cgs unit) (27), the stimulation should decrease the susceptibility difference from 3.8 to 1.6×10^{-8}. Modeling the cerebral vasculature as a set of randomly oriented cylinders (28), an initial blood volume of 4% should produce a 2% signal increase in GE images at TE = 40 ms. This prediction is in reasonable agreement with our empirical data. Since the effect of $\Delta\chi$ is more pronounced at high field strength (13, 29), higher-field imaging magnets will increase the observed T_2^* changes.

The observed activation response rise time for the GE images likely reflects the vascular transit times of the brain. Although oxygen exchange takes place at the capillary level, we would not expect to see the bulk of the activation-induced T_2^* change until the blood has transited the capillary bed and the (relatively) oxygenated blood fills the venous capacitance vessels. Our observed signal rise times ($\approx$4 s) are in reasonable agreement with the cerebrovascular transit times measured with ^{15}O-labeled carboxyhemoglobin (25). In addition, GE signal rise times are also consistent with previous optical imaging measurements of intrinsic cortical signal changes ("slow component") thought to reflect vascular oxygenation perturbations (30, 31).

In our experiments, we also observed signal changes on T_1-weighted inversion recovery images, similar in magnitude to those observed on T_2^*-weighted images. The relationship between T_1 and regional blood flow (see *Appendix*) was characterized by Detre *et al.* (14, 15):

$$1/T_{1_{app}} = 1/T_1 + f/\lambda, \qquad [1]$$

where the $T_{1_{app}}$ is the observed (apparent) longitudinal relaxation time with flow effects included, T_1 is the true tissue longitudinal relaxation time in the absence of flow, f is the flow in ml per g per unit time, and λ is the brain–blood partition coefficient of water [$\approx$0.95 ml/g (32)]. If we assume that the true tissue T_1 remains constant with stimulation, a change in blood flow Δf will lead to a change in the observed $T_{1_{app}}$:

$$\Delta(1/T_{1_{app}}) = \Delta(f/\lambda). \qquad [2]$$

Thus, the MR signal change can be used to estimate the change in blood flow. For an inversion recovery sequence with TI $\approx T_1$ and assuming constant proton density, a 2% change in MR signal intensity implies a change in flow (in conventional units) of ≈50 ml per 100 g per min (see *Appendix*). This change is in good agreement with previous PET measurements of blood flow increases during visual stimulation (2, 33–35). Of note, the rise-time constant for T_1-weighted signal changes with activation is longer than that observed with T_2^* imaging. Although one expects that the time to establish a magnetization equilibrium secondary to flow changes will be slower than the instantaneous hemodynamic response time [≤500 ms by optical techniques (30, 31)], our observed time constants are significantly longer than the $T_{1_{app}}$ time (≈1 s) implied by the model and equations of Detre *et al.* (14, 15). The long time constant observed may thus be physiologic in origin. Further experiments and improved modeling should aid in properly characterizing this behavior.

The experiments discussed above were limited to a single slice. However, this limit is not intrinsic but reflects memory limitations on our current, prototype system. With added computer memory, multiple-slice techniques, as well as true three-dimensional acquisitions, are possible with a temporal resolution of 3 s or less (19).

In general, a MR signal change in response to visual stimulation can be observed in a single image. To observe higher cognitive activation, which may be 5–10 times smaller than primary sensory activation, additional signal averaging could be used to achieve an equivalent signal/noise ratio. Under these conditions, gated imaging could be used to preserve temporal discrimination. In addition, improvements in rf coils and higher magnetic field strength imaging magnets should improve the fundamental contrast/noise ratio significantly.

The MR-based human brain activation studies reported here are intrinsically different from previous brain-mapping approaches and offer several advantages. First, the MRI techniques presented are completely noninvasive and, unlike our previous techniques (4), require no exogenous contrast medium. This means that imaging is repeatable over time within the same subject, allowing for intrasubject averaging. Intrasubject averaging is limited with radionuclide techniques such as PET, where human subject regulations prohibit multiple longitudinal or repeated studies across single subjects due to the buildup of radiation exposure. This is an important point, because many activation paradigms require averaging to achieve statistically significant results. The ability to repeat studies in a single subject offers the hope of understanding and quantifying individual variations in location and extent of activation for tasks too subtle to be studied with a single experiment. Given the inherent regional asymmetry of both anatomy and function (4, 36), intersubject averaging as used in PET imaging is thus fundamentally more limiting than the intrasubject averaging our technique allows.

Second, the temporal window offered by our technique provides tomographic imaging of human brain activity at a time scale similar to the hemodynamic response time. We have observed that in humans the onset and cessation of the hemodynamic response follows the task-induced neuronal activation. The only existing techniques with similar or better temporal resolution suitable for human use are electroencephalography or magnetoencephalography based, neither of which provides tomographic images.

The advent of MRI mapping techniques using intrinsic blood–tissue contrast promises development of a functional human neuroanatomy of unprecedented spatial–temporal resolution (37). In addition to three-dimensional localization of distributed processing centers, these techniques may allow for investigation of information processing at several levels of organization—ranging from neural systems to neural networks (18).

APPENDIX

In Detre *et al.* (15), the Bloch equation with tissue flow effect included describes the longitudinal magnetization as

$$\frac{dM_b}{dt} = \frac{M_b^0 - M_b}{T_1} + fM_a - \frac{f}{\lambda} M_b, \qquad \text{[A1]}$$

where M_b^0 = fully relaxed proton density of brain tissue; M_b = longitudinal magnetization of brain tissue; M_a = longitudinal magnetization of blood; T_1 = relaxation time of brain tissue in the absence of flow; f = blood flow; λ = blood brain partition coefficient. Hence,

$$\frac{dM_b}{dt} = \left(\frac{1}{T_1} + \frac{f}{\lambda}\right)\left(\frac{\frac{M_b^0}{T_1} + fM_a}{\frac{1}{T_1} + \frac{f}{\lambda}} - M_b\right). \qquad \text{[A2]}$$

From Eq. A2, we get apparent proton density M_{app}^0, where

$$M_{app}^0 = \frac{\frac{M_b^0}{T_1} + fM_a}{\frac{1}{T_1} + \frac{f}{\lambda}}, \qquad \text{[A3]}$$

and the brain magnetization M_b relaxes with an apparent T_1 time constant ($T_{1_{app}}$) given by

$$\frac{1}{T_{1_{app}}} = \frac{1}{T_1} + \frac{f}{\lambda}. \qquad \text{[A4]}$$

Note that Eq. A4 is independent of in-flow magnetization of M_a and holds under both the conditions of Detre *et al.* (15) and those described in this manuscript.

From Eq. A4, change in flow can therefore be measured directly from change in $T_{1_{app}}$

$$\Delta\left(\frac{f}{\lambda}\right) = \Delta\left(\frac{1}{T_{1_{app}}}\right). \qquad \text{[A5]}$$

It is possible to estimate flow change directly from signal change without actually measuring T_1 itself. In the case of no saturation or inversion of incoming arterial blood, as it was done in this manuscript, M_a can be replaced by M_b^0/λ, yielding $M_{app}^0 = M_b^0$. The proton density term remains unchanged. The MR signal acquired with the IR sequence becomes

$$M_b \propto 1 - 2e^{-TI/T_1} + e^{-TR/T_1}, \qquad \text{[A6]}$$

where M_b is MR signal intensity, TR is repetition time, TI is inversion recovery time interval. We can take the derivative ΔM_b with respect to $\Delta 1/T_1$

$$\frac{\Delta M_b}{M_b} = \frac{2TIe^{-TI/T_1} - TRe^{-TR/T_1}}{1 - 2e^{-TI/T_1} + e^{-TR/T_1}} \Delta\left(\frac{1}{T_1}\right). \qquad \text{[A7]}$$

Combining Eqs. A5 and A7, using TI $\approx T_1$, TR = 3.5 s, T_1 = 1.1 s, and our observed $\Delta M_b/M_b \approx 0.02$, we find

$$\Delta\left(\frac{f}{\lambda}\right) = \Delta\left(\frac{1}{T_1}\right) \approx 0.55/\text{min}. \quad \text{[A8]}$$

For $\lambda = 0.95, f \approx 0.5/\text{min}$.

Note Added in Proof. Recent results from our laboratory and other centers indicate that brain activation can be observed with conventional MR imaging, albeit with decreased temporal resolution (38).

We thank P. T. Fox for many helpful discussions and for the loan of the photic goggles. This work was presented in part at the Tenth Annual Meeting of the Society of Magnetic Resonance in Medicine, San Francisco, CA, August 10–16, 1991. This work was supported by grants from the National Institutes of Health (RO1-CA40303, RO1-HL39810, and 5PO1CA48729-02), the McDonnell-Pew Program in Cognitive Neuroscience, and General Electric Corp.

1. Zeki, S., Watson, J. D. G., Lueck, C. J., Friston, K. J., Kennard, C. & Frackowiak, R. S. J. (1991) *J. Neurosci.* **11**, 641–649.
2. Fox, P. T., Mintun, M. A., Raichle, M. E., Miezin, F. M., Allman, J. M. & Van Essen, D. C. (1986) *Nature (London)* **323**, 806–809.
3. Fox, P. T. & Raichle, M. E. (1986) *Proc. Natl. Acad. Sci. USA* **83**, 1140–1144.
4. Belliveau, J. W., Kennedy, D. N., McKinstry, R. C., Buchbinder, B. R., Weisskoff, R. M., Cohen, M. S., Vevea, J. M., Brady, T. J. & Rosen, B. R. (1991) *Science* **254**, 716–719.
5. Fox, P. T., Raichle, M. E., Mintun, M. A. & Dence, C. (1988) *Science* **241**, 462–464.
6. Phelps, M. E., Kuhl, D. E. & Mazziotta, J. C. (1981) *Science* **211**, 1445–1448.
7. Prichard, J., Rothman, D., Novotny, E., Petroff, O., Kuwabara, T., Avison, M., Howseman, A., Hanstock, C. & Shulman, R. (1991) *Proc. Natl. Acad. Sci. USA* **88**, 5829–5831.
8. Ogawa, S., Lee, T. M., Nayak, A. S. & Glynn, P. (1990) *Magn. Reson. Med.* **14**, 68–78.
9. Ogawa, S. & Lee, T. M. (1990) *Magn. Reson. Med.* **16**, 9–18.
10. Turner, R., Le Bihan, D., Moonen, C. T. W. & Frank, J. (1991) *J. Magn. Reson. Imaging* **1**, 227.
11. Turner, R., Le Bihan, D., Moonen, C. T. W., Despres, D. & Frank, J. (1991) *Magn. Reson. Med.* **22**, 159–166.
12. Hoppel, B. E., Weisskoff, R. M., Thulborn, K. R., Moore, J. B. & Rosen, B. R. (1991) in *Tenth Annual Meeting of the Society of Magnetic Resonance in Medicine* (SMRM, Berkeley), p. 308.
13. Thulborn, K. R., Waterton, J. C., Matthews, P. M. & Radda, G. K. (1982) *Biochim. Biophys. Acta* **714**, 265–270.
14. Detre, J. A., Leigh, J. S., Williams, D. S. & Koretsky, A. P. (1990) in *Ninth Annual Meeting of the Society of Magnetic Resonance in Medicine* (SMRM, Berkeley), p. 1289.
15. Detre, J. A., Leigh, J. S., Williams, D. S. & Koretsky, A. P. (1992) *Magn. Reson. Med.* **23**, 37–45.
16. Williams, D. S., Detre, J. A., Leigh, J. S. & Koretsky, A. P. (1992) *Proc. Natl. Acad. Sci. USA* **89**, 212–216, and Correction (1992) **89**, 4220.
17. Kwong, K. K., Belliveau, J. W., Stern, C., Chesler, D. A., Goldberg, I. E., Poncelet, B. P., Kennedy, D. N., Weisskoff, R. M., Cohen, M. S., Turner, R., Cheng, H.-M., Brady, T. J. & Rosen, B. R. (1992) in *Tenth Annual Meeting of the Society for Magnetic Resonance Imaging* (SMRI, Chicago) p. 76.
18. Churchland, P. S. & Sejnowski, T. J. (1988) *Science* **242**, 741–745.
19. Cohen, M. S. & Weisskoff, R. M. (1991) *Magn. Reson. Imaging* **9**, 1–37.
20. Mansfield, P. (1977) *J. Physics C* **10**, L55–L58.
21. Fox, P. T. & Raichle, M. E. (1984) *J. Neurophysiol.* **51**, 1109–1120.
22. Fox, P. T. & Raichle, M. E. (1985) *Ann. Neurol.* **17**, 303–305.
23. Belliveau, J. W., Rosen, B. R., Kantor, H. L., Rzedzian, R. R., Kennedy, D. N., McKinstry, R. C., Vevea, J. M., Cohen, M. S., Pykett, I. L. & Brady, T. J. (1990) *Magn. Reson. Med.* **14**, 538–546.
24. Deiber, M. P., Passingham, R. E., Colebatch, J. G., Friston, K. J., Nixon, P. D. & Frackowiak, R. S. J. (1991) *Exp. Brain Res.* **84**, 393–402.
25. Grubb, R. L., Raichle, M. E., Eichling, J. O. & Ter-Pogossian, M. M. (1974) *Stroke* **5**, 630–639.
26. Kwong, K. K., Hoppel, B. E., Weisskoff, R. M., Kiihne, S., Barrere, B., Moore, J. B., Poncelet, B. P., Rosen, B. R. & Thulborn, K. R. (1992) in *Tenth Annual Meeting of the Society for Magnetic Resonance Imaging* (SMRI, Chicago) p. 44.
27. Weisskoff, R. M. & Kiihne, S. (1992) *Magn. Reson. Med.* **24**, 375–383.
28. Weisskoff, R. M., Hoppel, B. E. & Rosen, B. R. (1992) in *Tenth Annual Meeting of the Society for Magnetic Resonance Imaging* (SMRI, Chicago) p. 77.
29. Brooks, R. A. & Di Chiro, G. (1987) *Med. Phys.* **14**, 903–913.
30. Grinvald, A., Lieke, E., Frostig, R. D., Gilbert, C. D. & Wiesel, T. N. (1986) *Nature (London)* **324**, 361–364.
31. Frostig, R. D., Lieke, E. E., Ts'o, D. Y. & Grinvald, A. (1990) *Proc. Natl. Acad. Sci. USA* **87**, 6082–6086.
32. Raichle, M. E., Eichling, J. O., Straatmann, M. G., Welch, M. J., Larson, K. B. & Ter-Pogossian, M. M. (1976) *Am. J. Physiol.* **230**, 543–552.
33. Mintun, M. A., Fox, P. T. & Raichle, M. E. (1989) *J. Cereb. Blood Flow Metab.* **9**, 96–103.
34. Lueck, C. J., Zeki, S., Friston, K. J., Deiber, M. P., Cope, P., Cunningham, V. J., Lammertsma, A. A., Kennard, C. & Frackowiak, R. S. J. (1989) *Nature (London)* **340**, 386–389.
35. Fox, P. T., Miezin, F. M., Allman, J. M., Van Essen, D. C. & Raichle, M. E. (1987) *J. Neurosci.* **7**, 913–922.
36. Perlmutter, J. S., Powers, W. J., Herscovitch, P., Fox, P. T. & Raichle, M. E. (1987) *J. Cereb. Blood Flow Metab.* **7**, 64–67.
37. Belliveau, J. W., Cohen, M. S., Weisskoff, R. M., Buchbinder, B. R. & Rosen, B. R. (1991) *J. Neuroimaging* **1**, 36–41.
38. Belliveau, J. W. (1992) in *Eleventh Annual Meeting of the Society of Magnetic Resonance in Medicine* (SMRM, Berkeley), in press.